

Experimental Petrology of the 1991–1995 Unzen Dacite, Japan. Part II: Cl/OH Partitioning between Hornblende and Melt and its Implications for the Origin of Oscillatory Zoning of Hornblende Phenocrysts

HIROAKI SATO^{1*}, FRANCOIS HOLTZ², HARALD BEHRENS², ROMAN BOTCHARNIKOV² AND SETSUYA NAKADA³

¹DEPARTMENT OF EARTH AND PLANETARY SCIENCES, FACULTY OF SCIENCE AND GRADUATE SCHOOL OF SCIENCE AND TECHNOLOGY, KOBE UNIVERSITY, KOBE, 657-8501 JAPAN

²INSTITUTE FOR MINERALOGY, UNIVERSITY OF HANNOVER, WELFENGARTEN 1, D-30167, HANNOVER, GERMANY

³EARTHQUAKE RESEARCH INSTITUTE, UNIVERSITY OF TOKYO, YAYOI 1-1-1, BUNKYO, TOKYO, 113-0032 JAPAN

RECEIVED NOVEMBER 10, 2002; ACCEPTED AUGUST 11, 2004
ADVANCE ACCESS PUBLICATION DECEMBER 10, 2004

High-temperature–pressure experiments were carried out to determine the chlorine–hydroxyl exchange partition coefficient between hornblende and melt in the 1992 Unzen dacite. Cl in hornblende and melt was analyzed by electron microprobe, whereas OH in hornblende and melt was calculated assuming anion stoichiometry of hornblende and utilizing the dissociation reaction constant for $H_2O + O = 2(OH)$ in water-saturated melt, respectively. The partition coefficient strongly depends on the $Mg/(Mg + Fe)$ ratio of hornblende, and is expressed as $\ln K_1 = (Cl/OH)_{hb}/(Cl/OH)_{melt} = 2.37 - 4.6[Mg/(Mg + Fe)]_{hb}$ at 2–3 kbar and 800–850°C. The twofold variation in Cl content in the oscillatory zoned cores of hornblende phenocrysts in the 1991–1995 dacite cannot be explained by the dependence of the Cl/OH partition coefficient on the $Mg/(Mg + Fe)_{hb}$ ratio, and requires c. 80% variation of the Cl/OH ratio of the coexisting melt. Available experimental data at 200 MPa on Cl/OH fractionation between fluid and melt suggest that c. 1.2–1.8 wt % degassing of water from the magma can explain the required 80% variation in the Cl/OH ratio of the melt. The negative correlation between Al content and $Mg/(Mg + Fe)$ ratio in the oscillatory zoned cores of the hornblende phenocrysts is consistent with repeated influx and convective degassing of the fluid phase in the magma chamber.

KEY WORDS: chlorine; element partitioning; hornblende; oscillatory zoning; Unzen volcano

INTRODUCTION

Compositional zoning in phenocryst minerals in volcanic rocks may record various magmatic processes. Oscillatory zoning has been interpreted as a consequence of kinetically controlled oscillation in crystal growth (e.g. Haase *et al.*, 1980), repeated replenishment of the magma chamber (e.g. Davidson & Tepley, 1997), intermittent turbulent mixing of the chamber by tidal oscillation (Anderson, 1984), and boundary layer convection and mixing (Nakada *et al.*, 1994). Patchy zoning (sieve texture) is another story and may be formed by rapid cooling (Kawamoto, 1992), rapid decompression (Nelson & Montana, 1992), or dissolution of crystals at hyperliquidus conditions (Nakamura & Shimakita, 1998). Minor element behaviour often helps to resolve the processes of compositional variation in minerals (e.g. Blundy & Shimizu, 1991), although there are possible effects of

*Corresponding author. Telephone: 81-78-803-5732. Fax: 81-78-803-5757. E-mail: hsaito@kobe-u.ac.jp

diffusion in modifying trace element zoning in minerals, as recently demonstrated for Mg in plagioclase (Costa *et al.*, 2003). During the course of petrographic examination of the 1991–1995 dacite of Unzen volcano, Japan, we observed oscillatory, patchy and reverse zoning in the hornblende phenocrysts in back-scattered electron images, which reflects the variation of Mg/(Mg + Fe) ratio in the hornblende. We further identified correlations among Cl, Al, Mg and Fe in the oscillatory zoned cores of the hornblende phenocrysts. The chlorine content of the oscillatory zoned cores of the hornblende phenocrysts in the Unzen dacite varies from 0.035 to 0.075 wt %.

Chlorine is strongly partitioned into any fluid phase separating from magmas (Shinohara, 1994), and, if the distribution coefficients between minerals and melt are known, can be utilized to reveal the degassing history of magmas through the analysis of chlorine zoning in Cl-bearing minerals. Icenhower & London (1997) experimentally determined the distribution coefficient of Cl and F between biotite and silicic melt at 800°C and 200 MPa, and showed their strong dependence on the Mg/(Mg + Fe) ratio of biotite. The strong effect of Mg/(Mg + Fe) ratio of biotite and hornblende on the distribution of Cl and F has been predicted from crystal-chemical considerations (Volfinger *et al.*, 1985; Oberti *et al.*, 1993); that is, the large anionic size of chlorine (181 pm; Shannon & Prewitt, 1969) is readily accommodated in the crystal lattice of Fe-rich biotite and amphibole.

In this study, we describe the compositional zoning of hornblende in the 1991–1995 Unzen dacite. Then, we present experimental results for partitioning of Cl–OH between hornblende and melt in dacitic systems. Based on the experimental results, we evaluate quantitatively the processes responsible for the Cl zoning observed in hornblende phenocrysts in the 1991–1995 Unzen dacite.

PETROGRAPHY AND PHASE CHEMISTRY OF HORNBLLENDE IN UNZEN DACITE

Host rocks

The 1991–1995 eruption of Unzen volcano was mostly effusive with extrusion of viscous magmas accompanied by numerous collapse-type pyroclastic flows. Only two vulcanian explosions were recorded in the early stages of the activity (Nakada *et al.*, 1999). Most of the samples are poorly vesiculated with porosity of 10–20 vol. %; however, bread-crust bombs and blocks from the vulcanian explosions of 8 and 11 June 1991 exhibit variable vesicularity, ranging from 0 to 70 vol. %. The eruption products are entirely dacitic in bulk-rock composition. SiO₂

contents vary from 64.5 to 66 wt %, and total phenocryst contents vary from 20 to 30 vol. % (Nakada & Motomura, 1999). Phenocryst phases include plagioclase, hornblende, biotite, quartz, apatite, magnetite, ilmenite, and trace amounts of augite and orthopyroxene. Groundmass constituents are pargasite, plagioclase, magnetite, ilmenite, apatite, orthopyroxene, augite and glass. Later eruption products in 1994–1995 contained silica minerals in the groundmass. The glass content of the groundmass varies from 50 to 80 vol. %. Phenocryst minerals often show compositional zoning; that is, oscillatory, spike (isolated zone in otherwise uniform core) and patchy zoning in the core, dusty and reverse zoning at the rim of plagioclase and hornblende phenocrysts, and reverse zoning (increase in Ti toward the rim) in magnetite (Nakamura, 1995; Nakada & Motomura, 1999). The reverse zoning at the rims of the phenocrysts of plagioclase, hornblende, and magnetite has been interpreted as evidence of magma mixing, which took place just before the eruption (Nakamura, 1995; Nakada & Motomura, 1999; Venezky & Rutherford, 1999; Holtz *et al.*, 2005).

Hornblende zoning

Hornblende phenocrysts range from 0.3 to 5 mm in length and 0.1 to 1 mm in width. They usually show idiomorphic crystal forms. In some cases, the hornblende phenocrysts are surrounded by a thin breakdown corona (width <20 µm in most cases) composed of plagioclase, pyroxenes, iron–titanium oxides, and glass. Hornblende phenocrysts contain inclusions of plagioclase, biotite, magnetite, ilmenite, pyrrhotite, apatite, zircon and glass. Compositional zoning of the hornblende phenocryst can be classified into oscillatory, spike or patchy zoning in the core, and reverse zoning at the rim. The boundary between the core and rim of the hornblende phenocrysts is generally sharp, but often showing irregular corroded features. The groundmass pargasite is 5–50 µm across and crystals are often skeletal and/or rounded (Sato *et al.*, 1999).

Figure 1 shows back-scattered electron images of hornblende phenocrysts in the 1991–1995 Unzen dacite. In the images, bright zones represent iron-rich compositions, and dark zones correspond to magnesium-rich areas. Out of 50 images of hornblende phenocrysts, 20% have reversely zoned Mg-rich rims (Fig. 1c and d), and 80% are without rims (Fig. 1a and b). The thickness of the rim is 5–30 µm, averaging *c.* 10 µm. In these zoned outer rims (Fig. 1d), the zoning is of normal character. Oscillatory zoning in the core of hornblende phenocrysts varies from 5 to 100 µm in width, mostly between 20 and 50 µm. The zones usually show inner Fe-rich (FeO 14.0–14.5%; MgO 12.6–14.0%) and outer Mg-rich parts (FeO 13.0–14.0%; MgO 14.0–14.8%). These parts show gradation as illustrated in the back-scattered electron

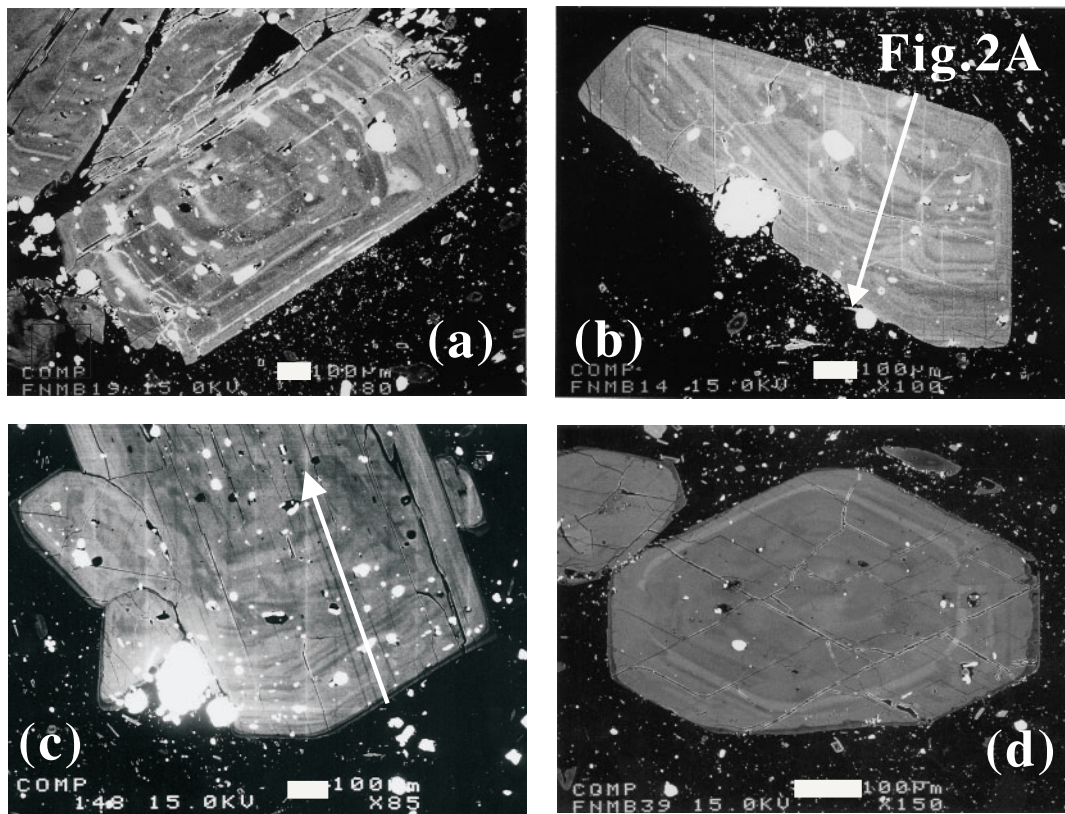


Fig. 1. Back-scattered electron images of hornblende phenocrysts in the 1991–1995 Unzen dacite. Scale bars represent 100 μm . (a) Bright zones are rich in Fe, and overgrow corroded, Mg-rich, dark zones. Sample 95101703-hb-3. (b) Oscillatory zoning often showing gradual transition from bright to dark zone and abrupt overgrowth of bright Fe-rich zone. Arrow shows the position of line scan shown in Fig. 2a. Sample 91K524E-hb-5. (c) Dark pargasitic rim of 20 μm thickness on Fe-rich oscillatory zoned core of hornblende phenocryst. Arrow shows the position of line scan of Fig. 2b. Sample 91K524E-hb-3. (d) Fe-rich ‘spike’ zone in otherwise fairly uniform core. The dark outer rim is corroded and encloses the crystal core. Sample 95101703A-hb-9.

images. The Fe-rich part often truncates the Mg-rich part of the inner zone (Fig. 1a and b). These textures are similar to the oscillatory zoning of plagioclase phenocrysts in the 1991–1995 Unzen dacite. In plagioclase phenocrysts, each zone shows a gradual decrease of $\text{Ca}/(\text{Ca} + \text{Na})$ ratio toward the outer part, which is often truncated by a new zone with high $\text{Ca}/(\text{Ca} + \text{Na})$ ratio. The correspondence of An-rich zones in plagioclase and iron-rich zones in hornblende cannot be explained by simple magmatic differentiation processes but suggests some other process, such as magma replenishment, for the formation of oscillatory zoning of the phenocrysts; this will be discussed subsequently.

Figure 2 shows examples of line analytical profiles across hornblende phenocrysts. In the line profiles, Mg is positively correlated with Si, and inversely correlated with Fe, Al, Na and Cl in the core of the phenocrysts (Fig. 2). This contrasts with the core–rim compositional change, where Mg is positively correlated with Al, Ti, Na and K, and negatively correlated with Si, Fe and Cl (left side of Fig. 2b). Major element correlations similar to

those observed in the core of oscillatory zoned hornblende phenocrysts in the Unzen dacite have been previously described from hornblende phenocrysts in the Fish Canyon Tuff by Bachmann & Dungan (2002).

Table 1 shows representative analyses of hornblende phenocrysts in the 1991–1995 Unzen dacite. The analytical conditions for the electron microprobe analyses are described in the legend to Table 1. Figure 3 shows compositional variations of Al vs $\text{Mg}/(\text{Mg} + \text{Fe})$ ratio. Within the oscillatory zoned cores of the amphiboles, Al is negatively correlated with $\text{Mg}/(\text{Mg} + \text{Fe})$ ratio (open symbols in Fig. 3). The amphibole rims have higher Al contents and $\text{Mg}/(\text{Mg} + \text{Fe})$ ratios when compared with the cores (Fig. 2b). The groundmass amphibole is pargasite (after Leake *et al.*, 1997) and has the same composition as the rims of the hornblende phenocrysts. Other oxides, such as Na, Ti and K, also show a positive correlation with $\text{Mg}/(\text{Mg} + \text{Fe})$ ratio for the core to rim relation, and a negative correlation with $\text{Mg}/(\text{Mg} + \text{Fe})$ ratio for the core oscillatory zoning. These observations suggest that different processes are required to explain the origin of

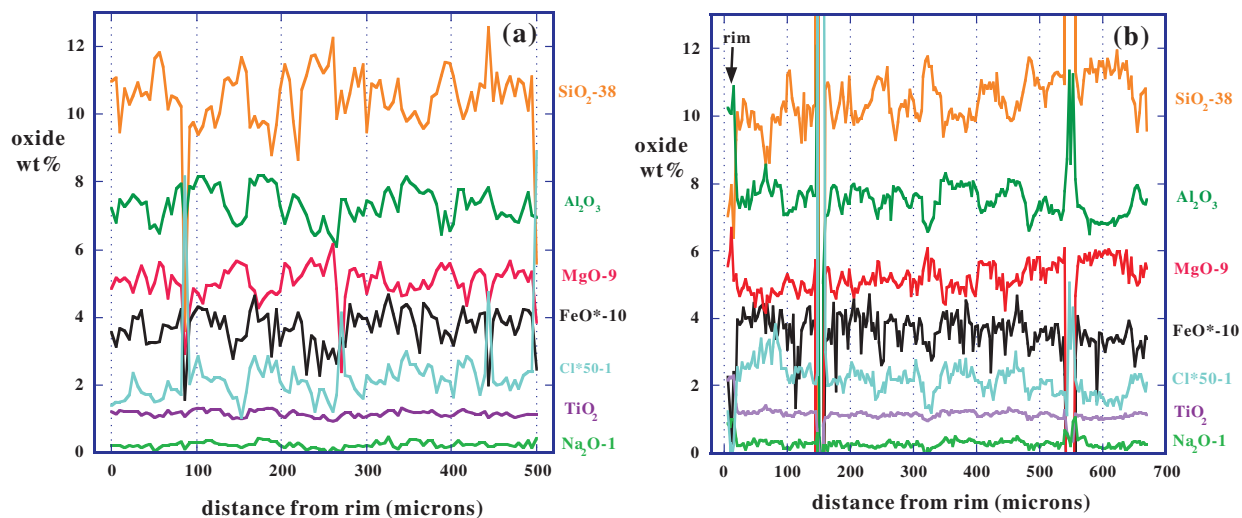


Fig. 2. Line profiles of hornblende phenocrysts in the 1991 Unzen dacite. Step interval of the analyses is 3.2 μm . Vertical scale is modified as shown on the right-hand side of each figure. In (a) the inverse correlation between Mg, Si and Al, Fe, Cl, Ti and Na in the core of the phenocryst should be noted. (b) The rim shows concomitantly high Al and Mg content, which is in contrast to the inverse correlation of Al and Mg in the core of the hornblende phenocryst. Position of the line scans is indicated in Fig. 1.

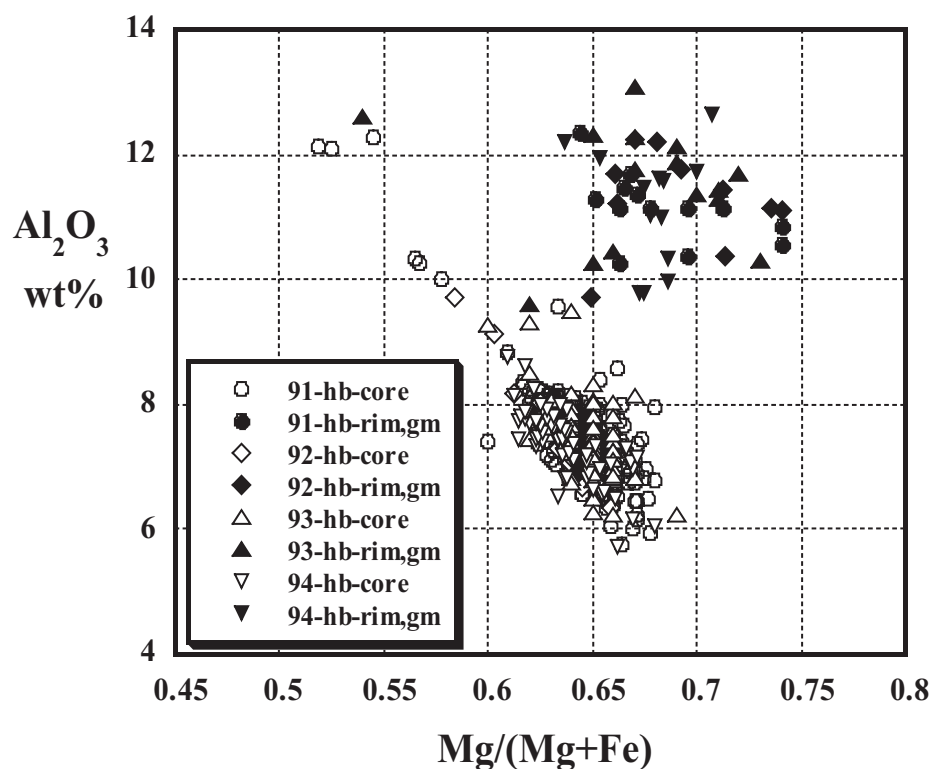


Fig. 3. Al_2O_3 wt % vs $\text{Mg}/(\text{Mg} + \text{Fe})$ of hornblende in the 1991–1995 Unzen dacite. Open symbols are analyses of hornblende cores. Filled symbols are analyses of hornblende rims (phenocrysts) and groundmass hornblende.

the compositional variations (1) within the cores and (2) between cores and rims of amphiboles. Figures 4 and 5 illustrate the chlorine content of hornblende phenocrysts. Figure 4 shows a positive correlation between Al_2O_3 and

Cl for the oscillatory zoned cores of the hornblende phenocrysts (varying from *c.* 0.035 to 0.075 wt % Cl), whereas the Cl content of the rims is markedly lower (0.01–0.02 wt % Cl). Figure 5 demonstrates a negative

Table 1: Representative compositions of hornblende in the 1991–1995 dacite of Unzen volcano

Sample:	uz-91K524			uz-92081301A			uz-95101705								
	hb-1-5 phen-c	hb-1-8 phen-c	hb-2-1 phen-c	gmhb-10 gm	gmhb-7 gm	hb-2-4 phen-c	hb-1-7 phen-c	hb-2-7 phen-c	gmhb-7 gm	gmhb-8 gm	hb-2-10 phen-c	hb-2-5 phen-c	hb-3-2 phen-c	gmhb-9 gm	gmhb-4 gm
SiO ₂	49.06	48.06	45.54	45.13	43.55	49.31	47.28	47.27	44.51	43.20	48.25	47.65	47.38	43.88	45.23
TiO ₂	1.05	1.32	1.77	2.43	2.31	1.07	1.20	1.30	2.58	2.58	1.50	1.09	1.30	2.41	2.16
Al ₂ O ₃	6.76	7.43	8.82	10.58	11.70	6.77	7.47	8.18	11.13	12.24	7.09	7.43	8.00	11.73	9.79
FeO*	14.03	14.37	14.50	9.81	12.12	14.00	14.27	14.77	9.55	12.23	13.06	14.21	14.20	11.33	12.57
MnO	0.52	0.56	0.49	0.12	0.18	0.47	0.48	0.48	0.17	0.15	0.37	0.51	0.49	0.22	0.25
MgO	14.59	13.69	12.64	15.72	13.69	14.68	13.87	13.10	14.91	13.92	14.76	13.80	13.88	14.82	14.67
CaO	10.97	10.95	11.04	11.05	11.40	11.04	11.20	11.26	11.05	11.59	10.73	11.26	11.21	11.24	11.18
Na ₂ O	1.15	1.18	1.37	1.86	1.82	1.17	1.16	1.22	1.85	2.01	1.70	1.29	1.31	2.12	1.78
K ₂ O	0.29	0.36	0.48	0.36	0.42	0.30	0.41	0.47	0.33	0.44	0.40	0.47	0.49	0.46	0.46
Cl	0.042	0.060	0.075	0.011	0.014	0.054	0.063	0.076	0.011	0.015	0.039	0.060	0.074	0.012	0.022
Total	98.45	97.98	96.72	97.08	97.19	98.85	97.42	98.13	96.09	98.38	97.90	97.77	98.31	98.22	98.10
Mg/(Mg + Fe)	0.65	0.63	0.61	0.74	0.67	0.65	0.63	0.61	0.74	0.67	0.67	0.63	0.64	0.70	0.68
O = 23															
Si	7.114	7.029	6.792	6.559	6.412	7.117	6.971	6.933	6.528	6.300	7.026	6.999	6.922	6.376	6.600
Al(IV)	0.886	0.971	1.208	1.441	1.588	0.883	1.029	1.067	1.472	1.700	0.974	1.001	1.078	1.624	1.400
Al(VI)	0.270	0.311	0.345	0.373	0.444	0.269	0.271	0.349	0.455	0.407	0.245	0.287	0.300	0.387	0.285
Ti	0.114	0.145	0.199	0.266	0.256	0.116	0.133	0.144	0.284	0.283	0.164	0.120	0.142	0.263	0.237
Fe	1.701	1.757	1.808	1.193	1.492	1.690	1.760	1.812	1.171	1.492	1.591	1.745	1.735	1.377	1.534
Mn	0.063	0.070	0.062	0.015	0.022	0.057	0.060	0.060	0.021	0.019	0.045	0.063	0.061	0.026	0.031
Mg	3.153	2.985	2.811	3.406	3.005	3.160	3.049	2.864	3.260	3.027	3.204	3.022	3.023	3.210	3.192
Ca	1.704	1.716	1.764	1.721	1.799	1.707	1.769	1.769	1.737	1.811	1.674	1.772	1.754	1.750	1.747
Na	0.324	0.335	0.395	0.524	0.518	0.326	0.332	0.346	0.527	0.567	0.481	0.368	0.370	0.597	0.503
K	0.053	0.067	0.091	0.067	0.079	0.055	0.078	0.087	0.062	0.082	0.074	0.088	0.091	0.085	0.086
Total	15.382	15.386	15.476	15.563	15.615	15.381	15.452	15.432	15.518	15.687	15.478	15.465	15.476	15.696	15.615
Cl	0.010	0.015	0.019	0.003	0.003	0.013	0.016	0.019	0.003	0.004	0.010	0.015	0.018	0.003	0.005

The electron microprobe analyses were made at 15 kV and 12 nA. Full ZAF correction was applied to the background corrected count ratio. The counting time was mostly 20 s at peak position with 10 s background on both sides of the peak, but for Cl and F analyses 100–150 s counting at the peak position and 50–75 s counting for background was used. Standard errors of Cl and F analyses are 0.003 and 0.03 wt %, respectively. The crystals were analyzed using a focused beam, but for glass analyses a beam diameter of c. 10 μm was used. Standards used for quantitative analyses are pure synthetic oxides for Si, Ti, Al, Fe, Mn and Mg; CaSiO₃ for Ca; NaCl for Na and Cl; and natural adularia for K. phen-c, phenocryst core; gm, groundmass.

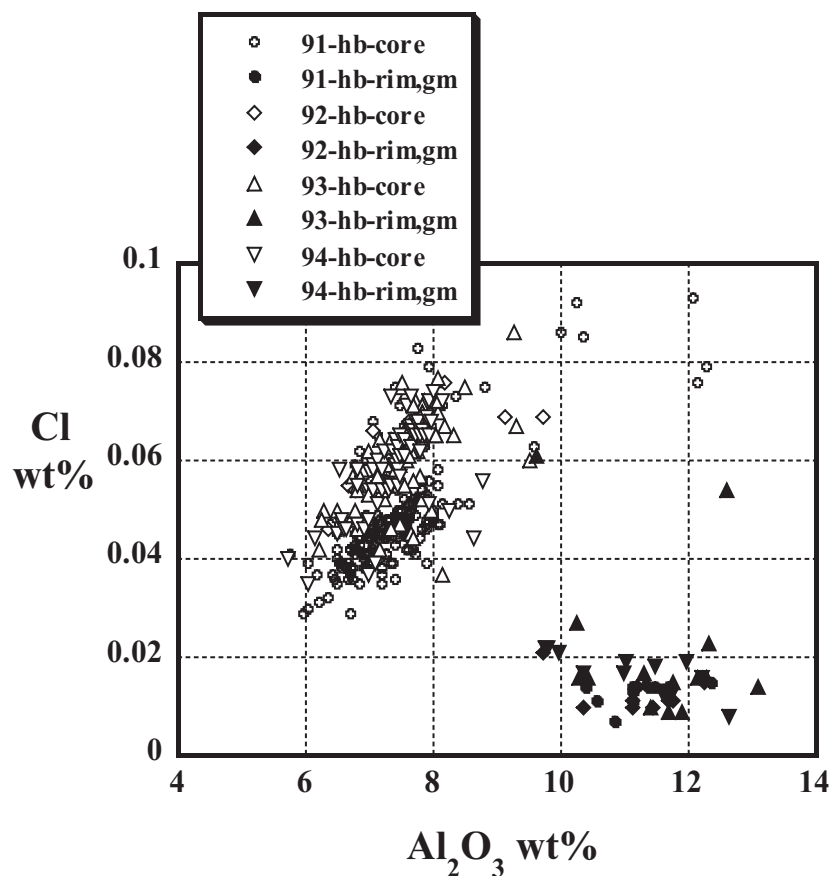


Fig. 4. Cl wt % vs Al_2O_3 wt % in hornblende phenocrysts and groundmass hornblende in the 1991–1994 Unzen dacite.

correlation between chlorine and $\text{Mg}/(\text{Mg} + \text{Fe})$ ratio for the cores and rims of hornblende but it can be observed that different compositional trends are observed for the cores and the rims. As noted previously, Cl is more readily accommodated by Fe-rich hornblende from a crystal-chemical viewpoint. However, we need a quantification of the compositional effects on the partition coefficient of Cl/OH between hornblende and melt to evaluate the origin of Cl zoning in hornblende phenocrysts.

EXPERIMENTAL STUDY

Experimental methods

Most of the high-pressure and -temperature partitioning experiments were carried out using externally heated pressure vessels at the University of Hannover. The experimental conditions were 200–300 MPa and 800–850°C. The oxygen fugacities of most of the charges were controlled at NNO (nickel–nickel oxide) buffer conditions by inserting Ni + NiO powder in a bomb consisting of a nickel alloy. The starting materials were glasses prepared by melting at *c.* 1600°C in air for 5 h of either

the bulk dacite or groundmass separates of the 1992 lava from Unzen. At this temperature, the $\text{Fe}^{3+}/(\text{total Fe})$ ratio is calculated to be 0.51–0.52 using the equation of Kilinc *et al.* (1983), which may have minimal effect on the redox state of the charge during the experiments. Some of the runs were carried out with FeO-doped starting materials. The compositions of the starting materials are shown in Table 2. The glass powder was inserted in Au or AgPd capsules together with NaCl or HCl aqueous solution. The concentration of NaCl or HCl in aqueous solution ranges from 2.5 to 11.2, mostly 4 wt %, and the amount of NaCl and HCl aqueous solution added to the charge ranges from 3.6 to 10.5 wt % (Table 3). The pressure was maintained at the nominal value monitored by a transducer, calibrated against a Heise gauge, and its uncertainty was within 5 MPa. The temperature was regulated by an automatic controller and is accurate to within 10 degrees. Experimental run duration was mostly 7 or 8 days (Table 3). The samples were quenched by cooling the bomb in air with *c.* 500°C drop of temperature within a minute. The run products were checked for possible volatile leakage both by weighing the capsule and by ensuring the presence of a vapor phase through

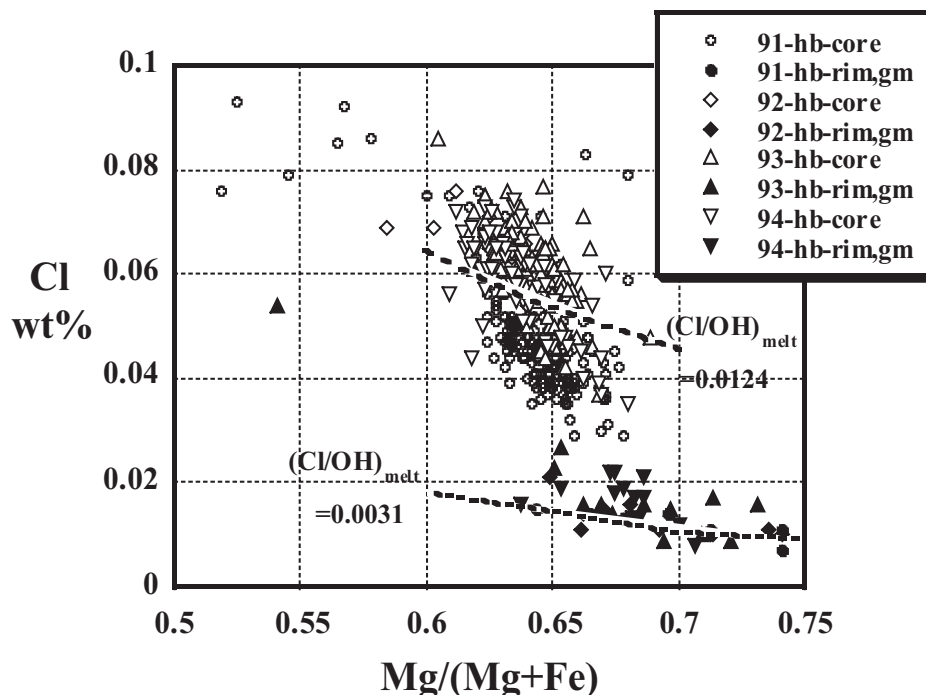


Fig. 5. Cl wt % vs Mg/(Mg + Fe) in hornblende phenocrysts and groundmass hornblende in the 1991–1995 Unzen dacite. Calculated compositional trends assuming constant Cl/OH ratios in the melt are shown as dashed curves (see text for details).

Table 2: Composition of starting materials for the element partition experiments

	UZBulk*	Fe-doped UZBulk†	Uzgm*	Fe-doped Uzgm†
SiO ₂	65.31	63.32	68.24	66.44
TiO ₂	0.66	0.58	0.53	0.47
Al ₂ O ₃	16.01	15.05	14.95	13.94
FeO	4.40	6.74	4.05	6.28
MnO	0.10	0.10	0.09	0.08
MgO	2.37	2.21	1.91	1.74
CaO	5.00	4.93	3.86	3.82
Na ₂ O	3.58	3.33	3.48	3.01
K ₂ O	2.40	2.41	2.85	3.00
P ₂ O ₅	0.16	0.27	0.14	0.17
Total	99.99	98.93	100.00	98.94

*XRF analyses.

†Electron microprobe analyses.

identifying the vapor leak during opening of the capsule after the run. The run products were mounted in epoxy resin and polished thin sections were prepared for optical and electron microprobe analyses.

The run conditions are listed in Table 3. Temperatures of the runs were either 800 or 850°C, and pressures were

185, 200 or 300 MPa. Table 4 lists the compositions of hornblende and glass in the run products, together with the standard error of the analyses. Most of the glass analyses gave totals of 92–95 wt %, which is consistent with the totals of H₂O-rich glass quenched from vapor-saturated conditions in the experimental runs. The SiO₂ content of the glass is in the range 69–76 wt % (anhydrous basis), and is similar to the estimated composition of the low-temperature Unzen end-member magma (prior to mixing) from which the hornblende phenocryst crystallized (Holtz *et al.*, 2005). Hornblende in the charge is, in a strict sense, classified mostly as edenite (after Leake *et al.*, 1997); i.e. Mg/(Mg + Fe) ratio is 0.47–0.71, Na + K p.f.u. is 0.38–0.72, Si p.f.u. is 6.92–7.37, and Al p.f.u. is 1.43–2.43.

Results

From the compositions of hornblende and glass (i.e. melt), we calculated the exchange partition coefficient of Cl and OH between hornblende and melt; i.e. $K_1 = (\text{Cl}/\text{OH})_{\text{hb}} / (\text{Cl}/\text{OH})_{\text{melt}}$. We used the water solubility model of Zhang (1999) to calculate the total water content in the melt. We neglected the presence of Cl in the vapor phase in calculating the water content of the melts, because the NaCl or HCl content of the aqueous solution added to the charge was fairly low (mostly 4 wt %). In calculating the OH content of the melt, the equilibrium constant for the dissociation reaction of water [$\text{H}_2\text{O} + \text{O} = 2(\text{OH})$] in

Table 3: Run conditions and phase assemblages of the experimental charges

No.	Capsule	Sample	Cl in fluid	NaCl or HCl (wt %)	Aqueous solution (wt %)	T ($^{\circ}\text{C}$)	P (MPa)	Duration (days)	$f\text{O}_2$	Phases in run products
278	Ag70Pd30	UZ Bulk Glass	NaCl	4	7.40	850	300	7	NNO	hb, mt, pl, gl
283	Ag70Pd30	UZ Bulk Glass	NaCl	4	7.10	850	300	7	NNO	hb, mt, pl, gl
286	Ag70Pd30	UZ Bulk Glass	NaCl	4	7.30	850	300	7	NNO	hb, mt, cpx, pl, gl
290	Au	UZ Bulk Glass	NaCl	4	5.20	850	300	7	NNO	hb, mt, pl, gl
291	Au	UZ Bulk Glass	NaCl	4	4.60	850	200	7	NNO	hb, mt, pl, gl
298	Au	Fe-doped UZ Bulk Glass	NaCl	4	3.60	800	300	7	NNO	hb, mt, opx, pl, gl
299	Au	Fe-doped UZ Bulk Glass	NaCl	4	4.10	850	200	7	NNO	hb, mt, opx, pl, gl
300	Au	Fe-doped UZ Bulk Glass	NaCl	4	4.85	850	300	7	NNO	hb, mt, pl, gl
307	Ag70Pd30	UZ Bulk Glass	NaCl	4	5.99	850	200	7	NNO	hb, mt, opx, pl, gl
309	Ag70Pd30	UZ Bulk Glass	NaCl	4	6.79	850	200	7	NNO	hb, mt, pl, gl
313	Ag70Pd30	Fe-doped UZ Bulk Glass	NaCl	4	6.88	850	300	7	NNO	hb, mt, pl, gl
314	Ag70Pd30	UZ Bulk Glass	NaCl	4	5.81	850	185	1	NNO + 4	hb, mt, gl
315	Ag70Pd30	UZ Bulk Glass	NaCl	4	4.55	850	185	1	NNO + 4	hb, mt, pl, gl
316	Ag70Pd30	Fe-doped UZ Bulk Glass	NaCl	4	6.49	850	185	1	NNO + 4	hb, mt, gl
320	Ag70Pd30	Fe-doped UZ Bulk Glass	NaCl	4	4.40	800	300	7	NNO	hb, mt, opx, pl, gl
322	Ag70Pd30	UZ GM Glass	NaCl	4	4.57	850	200	7	NNO	hb, opx, mt, pl, gl
323	Ag70Pd30	UZ GM Glass	NaCl	4	4.87	800	300	7	NNO	hb, opx, mt, pl, gl
324	Ag70Pd30	UZ GM Glass	NaCl	4	6.26	850	300	7	NNO	hb, mt, pl, gl
325	Ag70Pd30	UZ GM Glass	NaCl	4	3.75	800	200	7	NNO	hb, opx, pl, gl
326	Ag70Pd30	Fe-doped UZGM glass	NaCl	4	4.52	800	300	7	NNO	hb, mt, gl
329	Ag70Pd30	Fe-doped UZGM glass	NaCl	4	6.02	850	300	7	NNO	hb, mt, opx, gl
330	Ag70Pd30	UZ Bulk Glass	NaCl	4	4.61	850	200	7	NNO	hb, mt, opx, pl, gl
331	Ag50Pd50	UZ Bulk Glass	NaCl	4	4.43	800	300	7	NNO	hb, mt, opx, pl, gl
333	Ag70Pd30	Fe-doped UZBulk Glass	NaCl	4	5.15	850	200	7	NNO	hb, mt, opx, pl, gl
B51	Au	UZ GM Glass	HCl	2.8	9.83	850	200	5	NNO	hb, mt, opx, pl, gl
B52	Au	UZ GM Glass	HCl	5.6	10.02	850	200	5	NNO	hb, mt, opx, pl, gl
B53	Au	UZ GM Glass	HCl	11.2	10.30	850	200	5	NNO	hb, mt, opx, pl, gl
B57	Au	UZ GM Glass	HCl	2.8	10.05	850	300	5	NNO	hb, mt, gl
B58	Au	UZ GM Glass	HCl	5.6	10.15	850	300	5	NNO	hb, mt, gl
B59	Au	UZ GM Glass	HCl	11.2	10.46	850	300	5	NNO	hb, mt, gl

Runs 314, 315 and 316 were processed by internally heated pressure vessel at Kobe University; other runs were carried out by cold seal pressure vessel at the University of Hannover.

rhyolitic melts is adopted from Nowak & Behrens (2001), expressed as $\hat{K}_{\text{wd}} = 27.9 \exp(-4210/T)$, which was obtained by *in situ* high-temperature IR spectrometry. We supposed a stoichiometric concentration of anions in hornblende (two for $\text{O} = 23$) to calculate the amount of OH in hornblende, and anions other than chlorine were neglected. Fluorine was analyzed in some of the hornblende in the run products, but was found to be mostly in the range of 0–0.1 wt % with large relative errors, and may therefore be neglected in calculating the Cl/OH partition coefficient. The results of calculation of the partition coefficient are shown in Table 5. The partition coefficient K_1 varies from 0.32 to 1.53, and shows a

dependence on the $\text{Mg}/(\text{Mg} + \text{Fe})$ ratio of hornblende (Fig. 6). As noted previously, the partition coefficient may depend on the $\text{Mg}/(\text{Mg} + \text{Fe})$ ratio of hornblende based on crystal-chemical arguments (Oberti *et al.*, 1993). The least-squares regression line for $\ln K_1$ as a function of $\text{Mg}/(\text{Mg} + \text{Fe})_{\text{hb}}$ is: $\ln K_1 = 2.37 - 4.6[\text{Mg}/(\text{Mg} + \text{Fe})]_{\text{hb}}$ ($R = 0.82$). Compared with OH, Cl preferentially enters into hornblende with more iron-rich compositions [$\text{Mg}/(\text{Mg} + \text{Fe}) < 0.5$]. Other compositional parameters such as Al(IV), or $\text{Mg}/(\text{Mg} + \text{Fe}) \times \text{Al(IV)}$ as suggested by Sato *et al.* (1997), do not show good correlations with K_1 , and addition of these parameters to the regression does not improve the correlation coefficient. K_1 does not

Table 4: Phase compositions of the experimental run products

No.	phase/ <i>n</i>	SiO ₂	TiO ₂	Al ₂ O ₃	FeO	MnO	MgO	CaO	Na ₂ O	K ₂ O	Cl	Total
278	hb/10	45.20	2.24	10.84	13.86	0.22	12.90	11.14	1.80	0.61	0.021	98.83
		0.25	0.10	0.21	0.22	0.02	0.18	0.15	0.06	0.03	0.004	0.45
	gl/5	65.91	0.33	15.49	1.81	0.07	0.23	3.34	2.69	2.35	0.070	92.28
		0.61	0.02	0.42	0.08	0.02	0.04	0.30	0.19	0.04	0.008	0.45
283	hb/10	45.48	1.74	10.56	12.58	0.22	13.54	11.06	1.72	0.53	0.034	97.48
		0.75	0.25	0.51	0.52	0.03	0.35	0.18	0.07	0.04	0.003	1.02
	gl/6	65.61	0.36	15.33	2.69	0.09	0.59	3.55	3.09	2.67	0.124	94.09
		0.36	0.02	0.06	0.06	0.01	0.03	0.02	0.12	0.02	0.005	0.43
286	hb/11	47.85	1.10	8.26	14.07	0.46	13.99	11.07	1.34	0.53	0.053	98.72
		1.01	0.19	0.92	0.44	0.07	0.40	0.08	0.20	0.05	0.009	0.46
	gl/5	66.50	0.32	14.97	2.59	0.06	0.59	3.11	3.13	2.76	0.192	94.22
		0.21	0.02	0.10	0.14	0.02	0.05	0.05	0.14	0.02	0.008	0.36
290	hb/14	45.96	2.31	10.43	13.82	0.23	13.17	10.33	1.75	0.55	0.053	98.60
		0.63	0.23	0.30	0.58	0.03	0.51	0.18	0.10	0.04	0.005	0.69
	gl/5	67.19	0.27	14.19	2.20	0.09	0.38	3.08	2.85	2.83	0.184	93.24
		1.14	0.02	0.21	0.04	0.01	0.04	0.62	0.19	0.12	0.012	1.06
291	hb/13	46.41	2.32	9.60	13.94	0.23	11.97	10.57	1.75	0.52	0.066	97.37
		0.67	0.60	0.60	1.05	0.02	0.91	0.22	0.16	0.04	0.008	1.47
	gl/7	69.86	0.23	13.41	1.94	0.07	0.32	2.19	2.63	3.26	0.164	94.08
		0.18	0.02	0.08	0.08	0.01	0.02	0.06	0.17	0.10	0.007	0.41
298	hb/10	47.44	1.48	7.93	20.97	0.29	10.67	8.78	1.34	0.52	0.119	99.55
		0.91	0.13	0.84	1.16	0.06	0.41	0.58	0.13	0.14	0.014	0.73
	gl/5	72.74	0.15	12.39	1.75	0.04	0.19	1.72	2.63	3.99	0.180	95.78
		0.28	0.02	0.15	0.07	0.02	0.04	0.11	0.05	0.09	0.025	0.21
299	hb/1	45.68	1.80	9.31	17.54	0.25	12.18	9.65	2.02	0.54	0.066	99.02
		0.40	0.02	0.11	0.11	0.01	0.03	0.03	0.20	0.18	0.018	0.79
	gl/7	70.42	0.24	13.19	2.36	0.04	0.31	2.17	2.83	3.35	0.190	95.10
		0.40	0.02	0.11	0.11	0.01	0.03	0.03	0.20	0.18	0.018	0.79
300A	hb/5	44.08	1.98	9.96	20.35	0.14	10.76	9.52	1.76	0.47	0.084	99.12
		0.28	0.13	0.17	0.59	0.03	0.38	0.22	0.01	0.07	0.012	1.08
	gl/5	66.63	0.18	13.49	1.69	0.03	0.26	2.42	3.05	2.79	0.166	90.71
		0.32	0.02	0.09	0.07	0.02	0.01	0.06	0.13	0.02	0.002	0.43
307	hb/5	45.34	2.30	9.34	15.09	0.15	13.04	10.60	1.77	0.50	0.056	98.18
		0.77	0.17	0.22	0.47	0.08	0.43	0.26	0.02	0.04	0.003	0.48
	gl/4	65.16	0.33	13.44	1.68	0.04	0.40	2.93	2.91	2.95	0.171	90.01
		0.43	0.01	0.37	0.04	0.02	0.02	0.14	0.15	0.05	0.001	1.08
309	hb/5	45.53	2.22	9.12	14.93	0.14	13.97	10.25	1.70	0.45	0.043	98.36
		0.23	0.03	0.21	0.37	0.04	0.16	0.14	0.06	0.02	0.003	0.26
	gl/5	65.13	0.32	13.35	1.85	0.07	0.50	2.61	3.03	2.85	0.191	89.91
		0.53	0.02	0.19	0.13	0.02	0.11	0.19	0.19	0.12	0.007	0.93
313	hb/5	43.97	1.86	10.20	19.62	0.14	11.36	9.64	1.83	0.45	0.052	99.14
		0.47	0.07	0.41	0.82	0.03	0.24	0.17	0.05	0.03	0.001	0.96
	gl/5	65.11	0.19	13.73	1.95	0.03	0.33	2.71	3.10	2.60	0.186	89.94
		0.39	0.03	0.16	0.16	0.03	0.06	0.04	0.07	0.08	0.007	0.37
314	hb/10	44.10	1.40	12.26	11.14	0.25	13.50	11.74	1.69	0.58	0.051	96.71
		0.92	0.20	0.44	1.24	0.04	0.82	0.22	0.13	0.06	0.008	0.61
	gl/6	66.55	0.31	15.19	1.62	0.06	0.56	3.76	3.54	2.79	0.155	94.54
		0.50	0.06	0.15	0.22	0.03	0.02	0.07	0.26	0.04	0.005	0.35

Table 4: continued

No.	phase/n	SiO ₂	TiO ₂	Al ₂ O ₃	FeO	MnO	MgO	CaO	Na ₂ O	K ₂ O	Cl	Total
315	hb/7	44.69	1.91	12.97	10.46	0.22	12.77	11.27	1.88	0.71	0.055	96.93
		1.20	0.18	0.38	0.35	0.03	0.69	0.41	0.09	0.09	0.007	0.53
	gl/6	70.01	0.34	13.33	1.42	0.08	0.52	2.38	3.18	3.35	0.150	94.76
		1.23	0.02	0.91	0.18	0.02	0.06	0.39	0.27	0.07	0.011	0.72
316	hb/5	43.70	1.31	12.25	12.99	0.28	12.95	11.91	1.57	0.56	0.040	97.55
		0.42	0.15	0.30	1.70	0.08	0.90	0.13	0.08	0.03	0.005	0.37
	gl/6	66.19	0.29	15.23	1.49	0.05	0.58	3.86	3.63	2.68	0.157	94.15
		0.44	0.02	0.06	0.05	0.03	0.05	0.05	0.36	0.05	0.003	0.72
320	hb/8	45.16	2.04	9.26	19.52	0.22	9.83	9.71	1.54	0.63	0.087	98.00
		0.32	0.21	0.37	0.94	0.04	0.34	0.52	0.11	0.09	0.012	0.26
	gl/4	70.07	0.14	13.09	2.02	0.06	0.26	1.88	2.60	3.54	0.156	93.82
		0.73	0.02	0.40	0.13	0.04	0.03	0.09	0.18	0.09	0.009	0.37
322	hb/4	45.95	2.26	9.57	14.68	0.20	11.91	11.53	1.68	0.53	0.031	98.34
		0.84	0.33	1.22	0.26	0.05	0.44	1.06	0.21	0.06	0.003	0.75
	gl/3	68.92	0.29	13.82	2.33	0.06	0.43	2.61	2.72	3.24	0.124	94.54
		0.21	0.01	0.36	0.04	0.02	0.02	0.14	0.11	0.08	0.004	0.59
323	hb/3	46.14	1.63	9.63	17.57	0.31	10.94	9.86	1.57	0.55	0.062	98.26
		0.62	0.13	0.54	0.89	0.03	0.61	0.30	0.08	0.04	0.005	0.54
	gl/3	68.48	0.29	13.21	2.38	0.08	0.45	2.33	2.52	3.30	0.131	93.18
		0.84	0.09	0.02	0.33	0.01	0.15	0.27	0.15	0.09	0.008	0.36
324	hb/8	44.82	2.16	10.46	15.26	0.21	11.78	10.88	1.75	0.65	0.047	98.03
		0.45	0.22	0.48	0.62	0.02	0.83	0.15	0.08	0.07	0.004	0.59
	gl/3	65.99	0.30	14.62	2.91	0.08	0.53	3.21	2.75	2.82	0.153	93.36
		0.10	0.01	0.05	0.14	0.03	0.06	0.07	0.09	0.06	0.003	0.24
325	hb/2	46.73	1.57	9.22	16.86	0.21	10.11	10.28	1.60	0.54	0.067	97.19
		1.03	0.20	0.69	0.64	0.00	0.65	0.12	0.06	0.00	0.003	0.41
	gl/3	71.50	0.16	12.43	1.64	0.03	0.20	1.71	2.38	3.61	0.112	93.76
		0.63	0.01	0.00	0.06	0.02	0.01	0.09	0.01	0.15	0.004	0.81
326	hb/8	46.38	1.10	9.27	15.02	0.23	12.56	11.16	1.36	0.54	0.014	97.62
		0.81	0.13	0.40	1.40	0.02	0.80	0.38	0.07	0.05	0.004	0.36
	gl/3	67.82	0.14	13.91	2.16	0.07	0.37	2.85	2.59	2.80	0.039	92.75
		0.21	0.00	0.15	0.04	0.02	0.01	0.12	0.19	0.04	0.005	0.14
329	hb/1	45.60	1.46	8.66	16.93	0.21	12.46	10.90	1.41	0.44	0.036	98.09
		gl/5	67.37	0.21	14.18	3.15	0.06	0.51	3.15	2.79	2.90	0.140
			0.40	0.02	0.17	0.09	0.02	0.02	0.12	0.10	0.04	0.007
330	hb/2	46.80	2.11	10.36	12.50	0.20	12.32	10.94	1.81	0.57	0.048	97.67
		0.56	0.08	1.72	1.00	0.06	1.08	0.27	0.22	0.06	0.001	0.07
	gl/2	67.32	0.28	14.33	2.27	0.03	0.40	2.93	2.86	2.99	0.137	93.55
		0.59	0.00	0.84	0.19	0.03	0.01	0.54	0.26	0.19	0.008	0.69
331	hb/4	47.91	1.41	9.59	15.52	0.31	12.12	9.70	1.49	0.49	0.055	98.57
		0.20	0.14	0.78	0.04	0.04	0.49	0.26	0.11	0.03	0.001	0.57
	gl/6	71.09	0.16	12.76	1.46	0.04	0.20	1.82	2.41	3.33	0.134	93.40
		0.43	0.01	0.14	0.04	0.02	0.01	0.10	0.09	0.09	0.003	0.40
333	hb/3	44.73	1.49	10.40	16.91	0.16	11.92	10.08	1.70	0.55	0.037	97.97
		0.61	0.13	0.60	0.20	0.01	0.43	0.11	0.14	0.02	0.006	0.84
	gl/10	68.70	0.32	13.99	2.80	0.08	0.48	2.79	3.07	3.13	0.122	95.49
		0.39	0.02	0.08	0.11	0.02	0.03	0.08	0.09	0.11	0.005	0.53

No.	phase/ <i>n</i>	SiO ₂	TiO ₂	Al ₂ O ₃	FeO	MnO	MgO	CaO	Na ₂ O	K ₂ O	Cl	Total
B51	hb/10	47.73	1.77	9.31	13.34	0.38	12.60	10.72	1.35	0.51	0.072	97.78
		0.95	0.18	0.37	0.46	0.06	0.64	0.51	0.12	0.08	0.008	3.37
	gl/16	66.69	0.36	14.02	2.54	0.11	0.53	3.12	2.62	2.72	0.219	92.93
		0.19	0.02	0.12	0.21	0.04	0.04	0.10	0.15	0.06	0.011	0.93
B52	hb/6	46.56	1.84	8.34	13.25	0.35	14.63	10.81	1.28	0.34	0.084	97.47
		0.25	0.36	0.19	0.79	0.05	0.63	0.30	0.14	0.04	0.015	0.47
	gl/16	66.09	0.40	14.03	2.78	0.12	0.69	3.37	2.66	2.61	0.459	93.20
		0.23	0.02	0.13	0.13	0.04	0.04	0.08	0.09	0.06	0.013	0.82
B53	hb/6	46.37	1.73	8.82	13.25	0.35	14.57	10.58	1.16	0.32	0.106	97.25
		0.59	0.33	0.66	1.14	0.03	0.87	0.18	0.04	0.03	0.022	0.34
	gl/16	66.01	0.45	14.07	2.72	0.105	0.79	3.64	2.59	2.55	0.655	93.58
		0.36	0.02	0.13	0.13	0.046	0.04	0.10	0.22	0.08	0.015	0.36
B57	hb/10	47.43	1.75	8.60	13.81	0.34	13.09	10.97	1.24	0.45	0.052	97.75
		1.12	0.35	0.39	1.41	0.08	1.00	0.58	0.13	0.03	0.009	0.52
	gl/15	65.23	0.39	13.92	2.59	0.093	0.65	3.25	2.28	2.63	0.233	91.27
		0.33	0.03	0.14	0.16	0.048	0.04	0.10	0.39	0.08	0.006	0.39
B58	hb/6	47.10	1.35	7.83	14.07	0.42	14.22	10.88	1.14	0.32	0.079	97.40
		0.55	0.38	0.58	1.33	0.07	0.86	0.20	0.13	0.05	0.014	0.35
	gl/16	65.17	0.41	13.84	2.71	0.098	0.73	3.36	2.37	2.62	0.417	91.72
		0.30	0.01	0.12	0.09	0.057	0.04	0.09	0.11	0.06	0.009	0.39
B59	hb/6	47.51	1.67	7.98	11.88	0.34	16.07	10.32	1.10	0.30	0.087	97.26
		0.91	0.20	0.80	0.57	0.08	0.44	0.15	0.05	0.03	0.008	0.34
	gl/16	65.31	0.40	13.92	2.65	0.094	0.70	3.44	2.45	2.57	0.652	92.17
		0.32	0.02	0.14	0.12	0.053	0.05	0.07	0.12	0.08	0.015	0.43

n, number of analyses. Second line for each entry gives standard error of the analyses.

depend on pressure. The temperature effect on $\ln K_1$ is negative, and the following regression is obtained: $\ln K_1 = 8.62 - 3.46[\text{Mg}/(\text{Mg} + \text{Fe})]_{\text{hb}} - 0.0062T$, where T is the absolute temperature ($R = 0.80$). Although the data points in Fig. 6 show some scatter, mainly because of analytical errors in determining the compositions of phases, and possibly because of the assumption of the stoichiometric anionic contents of hornblende, we conclude that the most important controlling factor on the partition coefficient K_1 is the $\text{Mg}/(\text{Mg} + \text{Fe})$ ratio of hornblende.

DISCUSSION

Interpretation of chlorine variation in hornblende phenocrysts

In this section, we apply the newly derived partition coefficient to interpret the variation of chlorine content in hornblende phenocrysts in the Unzen dacite. As noted previously, the Cl content of hornblende is negatively correlated with the $\text{Mg}/(\text{Mg} + \text{Fe})$ ratio for both the core and rim (and groundmass) compositions. Figure 5

shows two dashed lines, which illustrate the calculated Cl content vs $\text{Mg}/(\text{Mg} + \text{Fe})$ ratio of hornblende assuming a constant Cl/OH ratio in the melt. The compositions of the rims (pargasite) mostly fit the lower dashed line with a molar $(\text{Cl}/\text{OH})_{\text{melt}}$ ratio of 0.0031, suggesting that these amphiboles crystallized from a melt with a nearly uniform molar Cl/OH ratio. On the other hand, the compositions of the phenocryst cores define a steeper slope than the calculated dashed line, which represents hornblende compositions in equilibrium with a melt of constant $(\text{Cl}/\text{OH})_{\text{melt}}$ ratio of 0.0124. The variation of the partition coefficient K_1 with the $\text{Mg}/(\text{Mg} + \text{Fe})$ ratio of the hornblende (Fig. 6) can account for *c.* 20% of the total variation in chlorine content of the cores of the hornblende phenocrysts; that is, *c.* 80% of the observed variations of chlorine content in the core of the hornblende phenocrysts should be ascribed to the variation of the Cl/OH ratio in the melt.

Cl/OH fractionation is probably caused by degassing of magmas and fluid input. We carried out incremental degassing calculations for melt compositions as illustrated in Fig. 7. The exchange partition coefficient of Cl/H₂O

Table 5: Calculation of partition coefficient of (Cl/OH) between hornblende and melt

Run	P (bar)	T (°C)	T (K)	K_{ws}	H ₂ O _t (wt %)	H ₂ O _t (mol)	H ₂ O _m	(OH) (mol)	Cl _m wt (wt %)	Cl _m (mol)	(Cl/OH) _m	(Cl/OH) _{amp}	K(Cl/OH) amp/melt	Mg-no. hb	Al(IV) hb
278	3000	850	1123-2	0.6592	0.074	0.126	0.0473	0.1574	0.00070	0.00061	0.00385	0.0028	0.727	0.624	0.945
283	3000	850	1123-2	0.6592	0.074	0.126	0.0473	0.1574	0.00124	0.00107	0.00681	0.0046	0.668	0.657	0.868
286	3000	850	1123-2	0.6592	0.074	0.126	0.0473	0.1574	0.00192	0.00166	0.01055	0.0069	0.657	0.639	0.680
290	3000	850	1123-2	0.6592	0.074	0.126	0.0473	0.1574	0.00184	0.00159	0.01011	0.0070	0.692	0.629	0.862
291	2000	850	1123-2	0.6592	0.059	0.102	0.0337	0.1358	0.00164	0.00144	0.01057	0.0088	0.835	0.605	0.730
298	3000	800	1073-2	0.55347	0.074	0.126	0.0509	0.1501	0.00180	0.00156	0.01038	0.0159	1.533	0.476	0.629
299	2000	850	1123-2	0.65909	0.059	0.102	0.0337	0.1358	0.00190	0.00166	0.01224	0.0088	0.722	0.553	0.844
300A	3000	850	1123-2	0.65909	0.074	0.126	0.0473	0.1574	0.00166	0.00144	0.00912	0.0115	1.258	0.485	0.976
307	2000	850	1123-2	0.65909	0.059	0.102	0.0337	0.1358	0.00171	0.00150	0.01102	0.0074	0.673	0.606	0.903
309	2000	850	1123-2	0.65909	0.059	0.102	0.0337	0.1358	0.00191	0.00167	0.01231	0.0056	0.459	0.625	0.918
313	3000	850	1123-2	0.65909	0.074	0.126	0.0473	0.1574	0.00186	0.00161	0.01022	0.0071	0.693	0.508	1.006
314	1850	850	1123-2	0.65909	0.056	0.097	0.0311	0.1311	0.00155	0.00136	0.01037	0.0069	0.666	0.684	0.975
315	1850	850	1123-2	0.65909	0.056	0.097	0.0311	0.1311	0.00150	0.00132	0.01004	0.0075	0.748	0.685	0.906
316	1850	850	1123-2	0.65909	0.056	0.097	0.0311	0.1311	0.00157	0.00138	0.01050	0.0055	0.520	0.640	1.035
320	3000	800	1073-2	0.55347	0.074	0.126	0.0509	0.1501	0.00156	0.00135	0.00899	0.0119	1.320	0.473	0.791
322	2000	850	1123-2	0.65909	0.059	0.102	0.0337	0.1358	0.00124	0.00109	0.00799	0.0041	0.516	0.591	0.825
323	3000	800	1073-2	0.55347	0.074	0.126	0.0509	0.1501	0.00131	0.00113	0.00755	0.0083	1.096	0.526	0.732
324	3000	850	1123-2	0.65909	0.074	0.126	0.0473	0.1574	0.00153	0.00132	0.00841	0.0063	0.746	0.579	0.908
325	2000	800	1073-2	0.55347	0.060	0.102	0.0371	0.1307	0.00112	0.00098	0.00750	0.0090	1.201	0.517	0.602
326	3000	800	1073-2	0.55347	0.074	0.126	0.0509	0.1501	0.00039	0.00034	0.00225	0.0018	0.813	0.599	0.737
329	3000	850	1123-2	0.65909	0.074	0.126	0.0473	0.1574	0.00140	0.00121	0.00769	0.0048	0.626	0.567	0.838
330	2000	850	1123-2	0.65909	0.059	0.102	0.0337	0.1358	0.00137	0.00120	0.00883	0.0063	0.714	0.637	0.713
331	3000	800	1073-15	0.55347	0.074	0.126	0.0509	0.1501	0.00134	0.00116	0.00772	0.0073	0.943	0.582	0.604
333	2000	850	1123-15	0.65909	0.059	0.102	0.0337	0.1358	0.00122	0.00107	0.00786	0.0050	0.631	0.557	0.892
B51	2000	850	1123-15	0.65909	0.059	0.102	0.0337	0.1358	0.00219	0.00192	0.01411	0.0095	0.675	0.627	0.628
B52	2000	850	1123-15	0.65909	0.059	0.102	0.0337	0.1358	0.00459	0.00402	0.02958	0.0112	0.377	0.663	0.800
B53	2000	850	1123-15	0.65909	0.059	0.102	0.0337	0.1358	0.00655	0.00573	0.04221	0.0141	0.334	0.662	0.806
B57	3000	850	1123-15	0.65909	0.074	0.126	0.0473	0.1574	0.00233	0.00202	0.01280	0.0068	0.533	0.628	0.676
B58	3000	850	1123-15	0.65909	0.074	0.126	0.0473	0.1574	0.00417	0.00361	0.02292	0.0104	0.453	0.643	0.719
B59	3000	850	1123-15	0.65909	0.074	0.126	0.0473	0.1575	0.00652	0.00564	0.03584	0.0114	0.317	0.707	0.737

K_{ws} denotes the equilibrium constant of the reaction $H_2O + O = 2(OH)$, calculated after Nowak & Behrens (2001). Water content of the melt is calculated after the method of Zhang (1999) assuming a water activity of one. (Cl/OH) ratio of hornblende was calculated assuming stoichiometry of the anion site on the basis of O = 23 neglecting other anions in the hornblende. t, total; m, melt; mol, molecular; amp, amphibole; Al(IV), Al in tetrahedral site in amphibole.

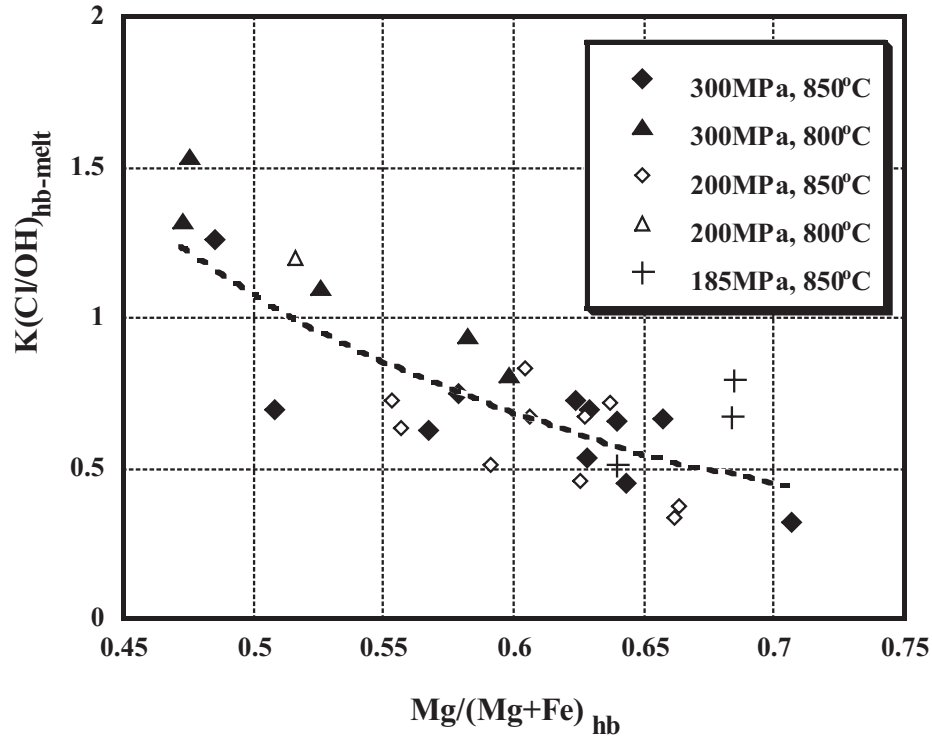


Fig. 6. Experimentally determined relationship between $K = (\text{Cl}/\text{OH})_{\text{hb}}/(\text{Cl}/\text{OH})_{\text{melt}}$ and $\text{Mg}/(\text{Mg} + \text{Fe})$ in hornblende. The dashed line represents the regression line for all the data points with the equation $K_1 = 10.67 \exp[-4.58(\text{Mg}/(\text{Mg} + \text{Fe})_{\text{hb}})]$ with $R = 0.82$.

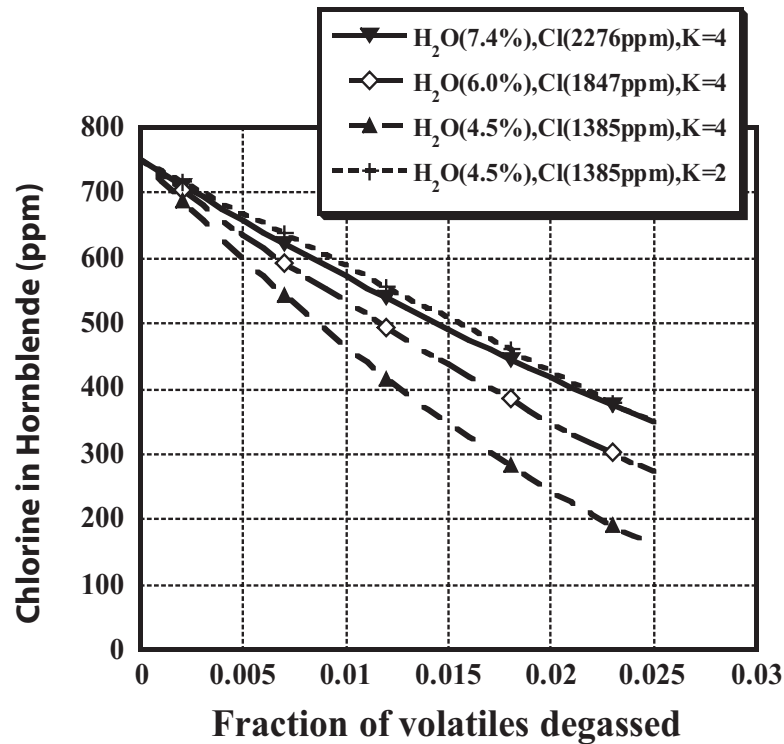


Fig. 7. Calculated variations of chlorine content of hornblende during degassing of magmas. K_1 is determined from Fig. 6. $K_2 = (\text{Cl}/\text{H}_2\text{O})_{\text{fluid}}/(\text{Cl}/\text{H}_2\text{O})_{\text{melt}}$ is varied between two and four based on the data of Webster (1992) at 200 MPa. Incremental fractional vesiculation by 0.1 wt % of water was assumed.

between fluid and melt at 200 MPa ranges from two to five based on the data of Webster (1992), and we adopted values of two and four for the degassing calculation. Figure 7 shows that about 70% of the variation in the Cl content of the hornblende requires 1.2–1.8 wt % degassing of H₂O from the magma. Thus, it is likely that during the crystallization of the oscillatory zoned cores of the hornblende phenocrysts, repeated degassing and fluid recharge of the magma took place.

Another possible cause of the change in (Cl/OH) melt ratio is the replenishment of the magma chamber by input of Cl-poor mafic magma and subsequent mixing of the magmas (Davidson & Tepley, 1997). This scenario, however, is not in agreement with the negative correlation between Al and Mg/(Mg + Fe) ratio observed in the oscillatory zoning of the hornblende phenocrysts. Replenishment of the magma chamber by mafic input will increase the Mg/(Mg + Fe) ratio and decrease the silica activity of the mixed magma, which may be reflected in concomitant increases of Mg/(Mg + Fe) ratio and Al content of hornblende such as observed in the reverse zoning of hornblende phenocrysts in Fig. 2b. Al in hornblende is affected by the composition of melt from which it crystallizes, and the following reaction indicates the increasing Al content of hornblende as a result of decrease of silica activity of the coexisting melt by magma replenishment: $\text{pargasite} + 4\text{SiO}_2 = \text{hornblende} + \text{albite}$ (e.g. Blundy & Holland, 1990). Decrease of silica activity shifts the reaction to the left-hand side of the equation, causing an increase in the Al content of the hornblende. Therefore, we should expect a positive correlation between Al and Mg/(Mg + Fe) ratio caused by replenishment of the magma chamber, which is opposite to the observed correlation in the oscillatory zoned cores of the hornblende phenocrysts. Therefore, the variation of Cl/OH as a result of magma replenishment is not a plausible mechanism for causing oscillatory zoning in the cores of the hornblende phenocrysts.

Convective degassing/fluid input in the chamber

Several arguments support the possibility of fluid input/degassing processes in the magma chamber to explain variations in the Cl content of hornblende. Generation of bubbles in a crystallizing mafic boundary layer in a stratified magma chamber has been proposed by Eichelberger (1980) as a mechanism for the formation of mafic inclusions. Simakin & Botcharnikov (2001) suggested that generation of bubbles in a stratified magma chamber may cause large-scale convective motion and mixing in the magma chamber, although Phillips & Woods (2002) argued that bubbles may separate and independently float up in the stratified chamber, and do not cause strong mixing in the magma chamber.

Murphy *et al.* (2000) and Couch *et al.* (2001) suggested the input of fluid and vesiculated mafic inclusions into the upper layer of a stratified magma chamber at Soufrière Hills Volcano, Montserrat. These models assume the generation of fluid of magmatic origin by crystallization-induced volatile oversaturation in a deep high-temperature mafic magma within a stratified magma chamber (Fig. 8b).

Another possible model was advocated by Hattori (1993) for the supply of sulfur in the silicic magma chamber at Pinatubo, in which uprising basic magma is saturated with a vapor phase, producing fluid pockets at the top of the mafic magma body. This fluid phase migrates along fractures towards the overlying silicic magma chamber as a result of buoyancy and the local stress field (Takada, 1994; Fig. 8a). Another possible source of the fluid is the heated meteoric water surrounding the lower magma chamber. The air-contaminated nature of the rare-gas isotopic composition of hornblende phenocrysts of the Unzen dacite (Hanyu & Kaneoka, 1997) supports a contribution of groundwater to the volatiles in the upper phenocryst-rich magma chamber. Input of fluid in this magma chamber results in the resorption of phenocrysts and a decrease in magma density triggers the convective uprise of magma in the chamber, which may vesiculate and degas at shallower depth. Degassing causes crystallization and an increase of magma density, and the degassed magma may descend in the chamber. Such fluid charge–convective degassing can occur repeatedly and oscillatory zoning of the phenocrysts may result. Equilibrium solubility of water in the dacitic melt at a depth of *c.* 11 km (*c.* 290 MPa) is *c.* 6.9 wt %, and at a depth of 8 km (210 MPa) is *c.* 5.8 wt %. These depths are indicated as pressure sources within the magma plumbing system beneath Unzen volcano by geodetic measurements (Ishihara, 1993; Nishi *et al.*, 1999). Although we are not fully convinced of the existence of large-scale convective motion in the magma chamber, the model of Kazahaya *et al.* (1994) that explains degassing of large amounts of sulfur dioxide in many active volcanoes—that is, convective degassing through the conduit and magma chamber—reinforces the above model of convective degassing in deep magma chambers. Degassed dense magmas find their way down the conduit into the magma chamber accompanied by an upwelling of low-density volatile-rich magma, which may eventually vesiculate and degas in a shallower part of the conduit or chamber (Fig. 8b).

This study has demonstrated that large variations in chlorine content in the oscillatory zones of hornblende phenocrysts in the 1991–1995 Unzen dacite are probably caused by fluid input–output processes in the magma chamber, based on the experimental determination of Cl/OH exchange partitioning between hornblende and melt. Although plagioclase phenocrysts in the 1991–1995

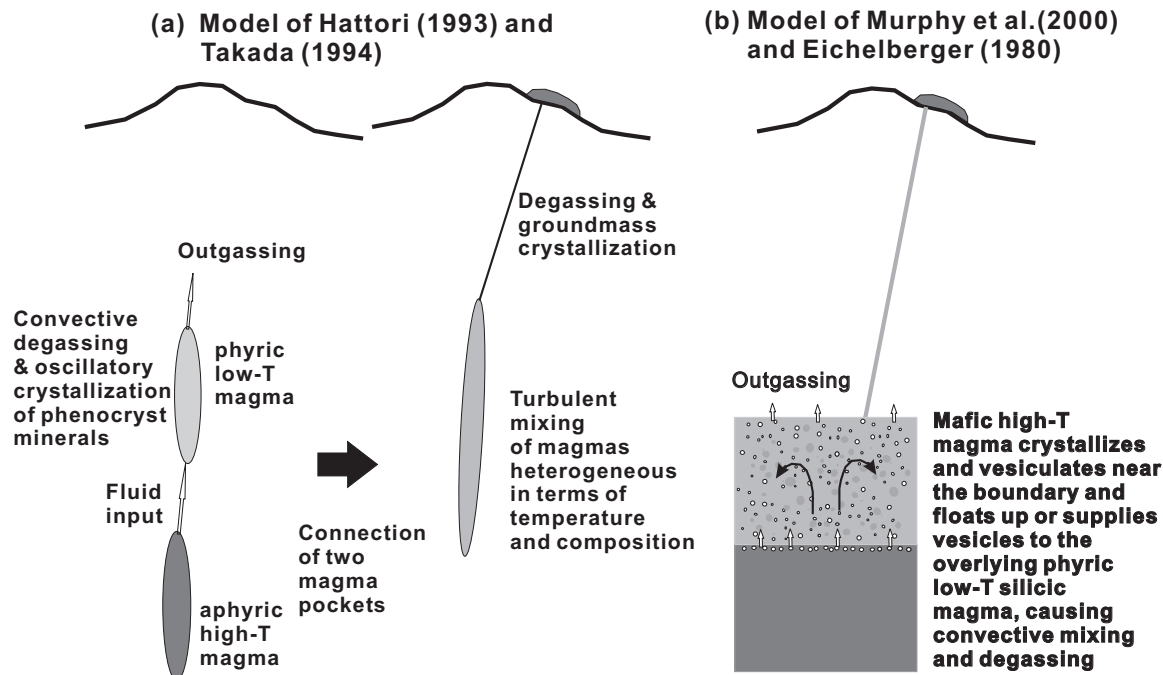


Fig. 8. Two possible models of fluid input–degassing explaining the chlorine zoning in the core of hornblende phenocrysts in the 1991–1995 Unzen dacite. (a) Chlorine is supplied from an uprising lower mafic magma chamber or heated surrounding saturated rocks into the upper phenocryst-rich magma chamber (Hattori, 1993), in which convective degassing takes place. The lower magma chamber may eventually connect to the upper magma chamber, which increases the uprise velocity (Takada, 1994) and initiates the eruption processes and mixing of magmas as recorded in the reverse zoning of the rims of hornblende phenocryst. (b) Crystallization-induced vapor saturation of the upper boundary of the lower mafic layer causes fluid and magma input into the overlying felsic layer of a stratified magma chamber as discussed by Eichelberger (1980), Murphy *et al.* (2000) and Couch *et al.* (2001).

dacite also show oscillatory, patchy, spike and reverse zoning, we have restricted the discussion to the origin of hornblende zoning, partly because there is rare-gas and Sr isotopic evidence for different sources for the hornblende and plagioclase phenocrysts in the Unzen dacite (Hanyu & Kaneoka, 1997; Chen *et al.*, 1999). Another problem for interpreting the oscillatory zoning of plagioclase as suggested by Costa *et al.* (2003). We need further experimental studies and analyses to resolve these aspects of the origin of oscillatory zoning of phenocryst minerals in volcanic rocks.

ACKNOWLEDGEMENTS

We appreciate discussions with Professor Wilhelm Johannes, Dr Youxue Zhang, Dr Atsushi Goto, Dr Susanne Ohlhorst and Dr Keiko Suzuki-Kamata. We also acknowledge technical assistance by Dr Jürgen Koepke, the late Dr Dieter Ziegenbein, Mr Otto Dietrich and other technical staff at the Institute for Mineralogy, University of Hannover. The paper benefited considerably from the critical reviews of Drs J. Barclay,

M. Rutherford and Ian Smith, and from the final improvements of Dr J. Gamble. Financial support came from the Unzen Scientific Drilling Project, MECSST, Japan, the DFG projects Ho1337/7 and Ho1337/11, and JSPS project 14340162.

REFERENCES

- Anderson, A. T. (1984). Probable relations between plagioclase zoning and magma dynamics, Fuego volcano, Guatemala. *American Mineralogist* **69**, 660–676.
- Bachmann, O. & Dungan, M. A. (2002). Temperature-induced Al-zoning in hornblendes of the Fish Canyon magma, Colorado. *American Mineralogist* **87**, 1062–1076.
- Blundy, J. D. & Holland, T. J. B. (1990). Calcic amphibole equilibria and a new amphibole–plagioclase geothermometer. *Contributions to Mineralogy and Petrology* **104**, 208–224.
- Blundy, J. D. & Shimizu, N. (1991). Trace element evidence for plagioclase recycling in calc-alkaline magmas. *Earth and Planetary Science Letters* **102**, 178–197.
- Chen, C. H., Nakada, S., Shieh, Y.-N. & DePaolo, D. J. (1999). The Sr, Nd and O isotopic studies of the 1991–1995 eruption at Unzen, Japan. *Journal of Volcanology and Geothermal Research* **89**, 243–253.
- Costa, F., Chakraborty, S. & Dohmen, R. (2003). Diffusion coupling between trace and major elements and a model for calculation of

- magma residence times using plagioclase. *Geochimica et Cosmochimica Acta* **67**, 2189–2200.
- Couch, S., Sparks, R. S. J. & Carroll, M. R. (2001). Mineral disequilibrium in lavas explained by convective self-mixing in open magma chambers. *Nature* **411**, 1037–1039.
- Davidson, J. P. & Tepley, F. J., III (1997). Recharge in volcanic systems: evidence from isotope profiles of phenocrysts. *Science* **275**, 826–829.
- Eichelberger, J. C. (1980). Vesiculation of mafic magmas during replenishment of silicic magma reservoirs. *Nature* **288**, 446–450.
- Haase, C. S., Chadam, J., Feinn, D. & Ortoleva, P. (1980). Oscillatory zoning in plagioclase feldspar. *Science* **288**, 272–274.
- Hanyu, T. & Kaneoka, I. (1997). Magmatic processes revealed by noble gas signatures: the case of Unzen volcano, Japan. *Geochemical Journal* **31**, 395–405.
- Hattori, K. (1993). High-sulfur magma, a product of fluid discharge from underlying mafic magma: evidence from Mount Pinatubo, Philippines. *Geology* **21**, 1083–1086.
- Holtz, F., Sato, H., Lewis, J., Behrens, H. & Nakada, S. (2005). Experimental petrology of the 1991–1995 Unzen dacite, Japan. Part 1: phase relations, phase composition and pre-eruptive conditions. *Journal of Petrology* **46**, 000–000.
- Icenhower, J. P. & London, D. (1997). Partitioning of fluorine and chlorine between biotite and granitic melt: experimental calibration at 200 MPa H₂O. *Contributions to Mineralogy and Petrology* **127**, 17–29.
- Ishihara, K. (1993). Continuous magma supply inferred from discharge rate of magma and ground deformation rate at Mt. Unzen, Japan. *Annals of the Disaster Prevention Research Institute, Kyoto University* **36**, 219–230 (in Japanese with English abstract).
- Kawamoto, T. (1992). Dusty and honeycomb plagioclase: indicators of processes in the Uchino stratified magma chamber, Izu Peninsula, Japan. *Journal of Volcanology and Geothermal Research* **49**, 191–208.
- Kazahaya, K., Shinohara, H. & Saito, G. (1994). Excessive degassing of Izu–Oshima volcano: magma convection in a conduit. *Bulletin of Volcanology* **56**, 207–216.
- Kilinc, A., Carmichael, I. S. E., Rivers, M. L. & Sack, R. O. (1983). The ferric–ferrous ratio of natural silicate liquids equilibrated in air. *Contributions to Mineralogy and Petrology* **83**, 136–140.
- Leake, B. E., Woolley, A. R., Birch, W. D., *et al.* (1997). Nomenclature of amphiboles—Report of the subcommittee on Amphiboles of the International Mineralogical Association Commission on New Minerals and Mineral Names. *European Journal of Mineralogy* **9**, 623–651.
- Murphy, M. D., Sparks, R. S. J., Barclay, J., Carroll, M. R. & Brewer, T. S. (2000). Remobilization of andesite magma by intrusion of mafic magma at the Soufrière Hills volcano, Montserrat, West Indies. *Journal of Petrology* **41**, 21–42.
- Nakada, S. & Motomura, Y. (1999). Petrology of the 1991–1995 eruption at Unzen: effusion pulsation and groundmass crystallization. *Journal of Volcanology and Geothermal Research* **89**, 173–196.
- Nakada, S., Bacon, C. R. & Gartner, A. E. (1994). Origin of phenocrysts and compositional diversity in pre-Mazama rhyodacite lavas, Crater Lake, Oregon. *Journal of Petrology* **35**, 127–162.
- Nakada, S., Shimizu, H. & Ohta, K. (1999). Overview of the 1990–1995 eruption at Unzen volcano. *Journal of Volcanology and Geothermal Research* **89**, 1–22.
- Nakamura, M. (1995). Continuous mixing of crystal mush and replenished magma in the ongoing Unzen eruption. *Geology* **23**, 807–810.
- Nakamura, M. & Shimakita, S. (1998). Dissolution origin and syn-entrapment compositional change of melt inclusion in plagioclase. *Earth and Planetary Science Letters* **161**, 119–133.
- Nelson, S. T. & Montana, A. (1992). Sieve-textured plagioclase in volcanic rocks produced by rapid decompression. *American Mineralogist* **77**, 1242–1249.
- Nishi, K., Ono, H. & Mori, H. (1999). Global positioning system measurement of ground deformation caused by magma intrusion and lava discharge: the 1990–1995 eruption at Unzendake volcano, Kyushu, Japan. *Journal of Volcanology and Geothermal Research* **89**, 23–34.
- Nowak, M. & Behrens, H. (2001). Water in rhyolitic magmas: getting a grip on a slippery problem. *Earth and Planetary Science Letters* **184**, 515–522.
- Oberti, R., Ungaretti, L., Cannillo, E. & Hawthorne, F. C. (1993). The mechanism of Cl incorporation in amphibole. *American Mineralogist* **78**, 746–752.
- Phillips, J. C. & Woods, A. W. (2002). Suppression of large-scale magma mixing by melt–volatile separation. *Earth and Planetary Science Letters* **204**, 47–60.
- Sato, H., Yamaguchi, Y. & Makino, S. (1997). Cl incorporation into successively zoned amphiboles from the Ramnes cauldron, Norway. *American Mineralogist* **82**, 316–324.
- Sato, H., Nakada, S., Fujii, T., Nakamura, M. & Suzuki-Kamata, K. (1999). Groundmass pargasite in the 1991–1995 dacite of Unzen volcano, Japan: experimental phase stability relations and its volcanological implications. *Journal of Volcanology and Geothermal Research* **89**, 197–212.
- Shannon, R. D. & Prewitt, C. T. (1969). Effective ionic radii in oxides and fluorides. *Acta Crystallographica* **B25**, 925–946.
- Shinohara, H. (1994). Exsolution of immiscible vapor and liquid phases from a crystallizing silicate melt: implications for chlorine and metal transport. *Geochimica et Cosmochimica Acta* **58**, 5215–5221.
- Simakin, A. G. & Botcharnikov, R. E. (2001). Effects of compositional convection at degassing of stratified magma. *Journal of Volcanology and Geothermal Research* **105**, 207–224.
- Takada, A. (1994). Development of a subvolcanic structure by the interaction of liquid-filled cracks. *Journal of Volcanology and Geothermal Research* **61**, 207–224.
- Venezky, D. Y. & Rutherford, M. J. (1999). Petrology and Fe–Ti oxide reequilibration of the 1991 Mount Unzen mixed magma. *Journal of Volcanology and Geothermal Research* **89**, 213–230.
- Volfinger, M., Robert, J.-L., Vielzeuf, D. & Neiva, A. M. R. (1985). Structural control of the chlorine content of OH-bearing silicates (mica and amphiboles). *Geochimica et Cosmochimica Acta* **49**, 37–48.
- Webster, J. D. (1992). Fluid–melt interactions involving Cl-rich granites: experimental study from 2–8 kbar. *Geochimica et Cosmochimica Acta* **56**, 659–678.
- Zhang, Y. (1999). H₂O in rhyolitic glasses and melts: measurement, speciation, solubility, and diffusion. *Reviews of Geophysics* **37**, 493–516.